Millisecond Curing Time of a Molecular Adhesive Causes Velocity-Dependent Cargo-Loading of Molecular Shuttles

Ashutosh Agarwal, Parag Katira, and Henry Hess*

Department of Materials Science and Engineering, University of Florida, Gainesville, Florida 32611-6400

ABSTRACT

It has been recently discovered that biological systems exploit complex intermolecular bonds, such as the "catch bond" between FimH proteins and mannose, to regulate dynamic assembly processes. Here we show that the assembly of hybrid nanostructures also has to account for and ideally exploit the subtleties of the utilized intermolecular interactions. We focus on the biotin–streptavidin bond, which gains its ultimate strength on a time scale of milliseconds, due to existence of metastable binding states. As a consequence of the gluelike character of this widely used intermolecular bond, the velocity of molecular shuttles, active nanoscale transport systems based on biomolecular motors and their associated filaments, has to be optimized to permit efficient attachment of cargo via biotin–streptavidin linkages. The attachment process can only be understood by combining rigorous mechanical engineering analysis with detailed physicochemical models.

The attachment of nanoscale cargo to motor protein-powered molecular shuttles is a key functional element of the overall design.[1,2] Several studies have explored the influence of cargo type, size, and density[3–9] as well as of different linkages, including biotin–streptavidin, cyclodextrin host–guest,[10] malachite green–aptamer,[11] DNA–DNA,[12] and antibody–antigen.[13–15] Here, we investigate for the first time the effect of shuttle velocity on cargo attachment via biotin–streptavidin linkages and discover an unexpected optimum in the shuttle velocity. We find that, similar to dynamic effects introduced by other complex intermolecular bonds such as the "catch bond" between FimH proteins and mannose[16] or P-selectin and P-selectin glycoprotein ligand-1,[17] this dynamic effect originates from the gluelike character of the biotin–streptavidin bond.

In the experiments (Figure 1), kinesin motor proteins are adsorbed to a surface precoated with casein; biotinylated microtubules adhere to the kinesin and are subsequently coated with rhodamine-labeled streptavidin. The microtubule gliding velocity was controlled via the concentration of the kinesin substrate ATP and varied between 50 and 450 nm/s. Finally, biotinylated fluorescein-labeled nanospheres were added in concentrations ranging from 25 to 100 pM, which resulted in surface densities of 250 to 2000 nanospheres within a field of view of the fluorescence microscope (80 μm × 80 μm). The nanospheres bound to kinesin-coated surfaces but not to surfaces coated only with casein.
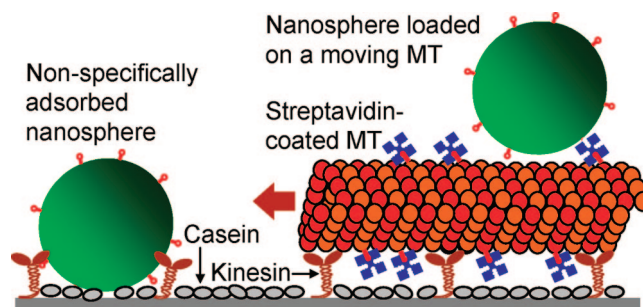

Figure 1. Sketch of principle. Biotinylated microtubules are coated with rhodamine-labeled streptavidin. Biotinylated fluorescein-labeled polystyrene nanospheres (40 nm diameter) adhere to the surface and attach to the streptavidin-coated microtubules as they move on the kinesin-coated surface.

Nanospheres attached to microtubules only as a result of collisions between gliding microtubules and nanospheres adhering to the surface. Binding of nanospheres from solution to moving microtubules was never observed, and stationary microtubules (in the absence of ATP) did not capture nanospheres from solution.

The attachment and subsequent transport of fluorescein-labeled, biotinylated nanospheres by microtubules coated with rhodamine-labeled streptavidin can be visualized by fluorescence microscopy, since loaded nanospheres appear as a distinct group of moving nanospheres colocalized with a moving microtubule. Control experiments were carried out in which 10% rhodamine- and 90% biotin-labeled microtubules were used but the streptavidin coating step was

* To whom correspondence should be addressed. E-mail: hhess@mse.ufl.edu. Fax: (352) 846-3355. Tel: (352) 846-3781.
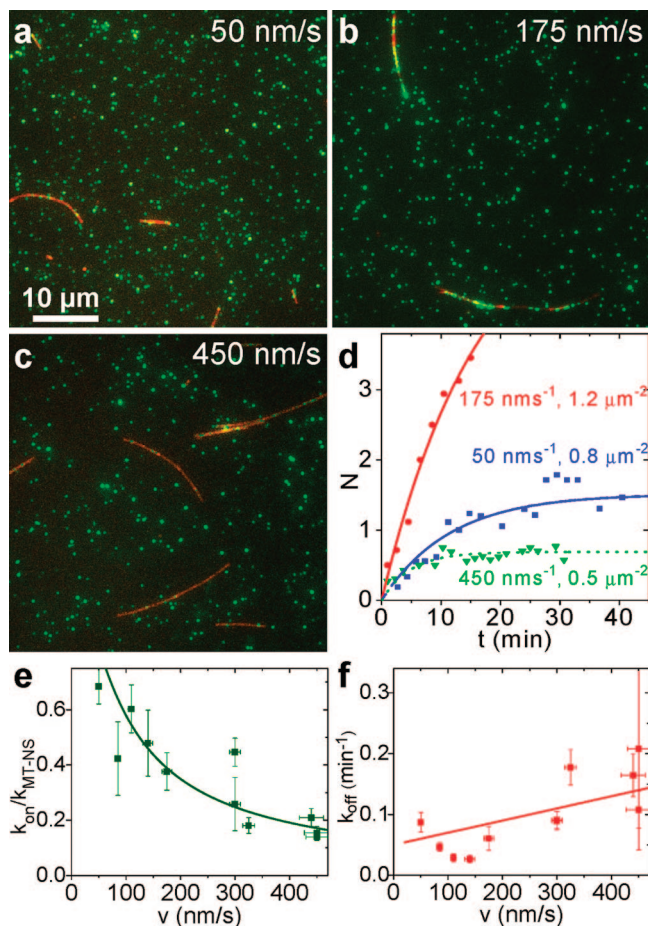
Figure 2. Experimental results. Loading of microtubules (false-colored red) moving at 50 nm/s (a), 175 nm/s (b) and 450 nm/s (c) 10 min after the injection of nanospheres (false-colored green). (d) The number of nanospheres loaded per microtubule graphed as a function of the time elapsed since bead injection (three data sets shown; all eleven data sets are included in the Supporting Information). Curves represent the fits of the data to eq 1 to generate attachment and detachment rates. (e) Attachment rates k_{on} as a function of microtubule velocity. (f) Detachment rates k_{off} as function of microtubule velocity. In panels e and f, the data points represent the fit parameters obtained from panel d while curves represent the theoretical model developed both for the attachment and detachment process.

omitted. These microtubules did not bind any nanosphere, which proves that the binding of nanospheres occurred specifically through the streptavidin–biotin chemistry. A striking dependence of nanosphere attachment on microtubule velocity was observed (Figure 2). The loading initially increases with velocity and reaches a maximum at a velocity ~200 nm/s, after which it decreases.

To gain a quantitative understanding of this unexpected observation, the number, N, of nanospheres loaded per microtubule was recorded as a function of time, t, after bead injection for different nanosphere concentrations and microtubule velocities (Figure 2d, details in Supporting Information). These data were modeled under the assumptions that cargo loading onto microtubules is reversible, that cargo attachment is a zero order reaction (because of large excess of vacant binding sites on microtubules and negligible decline in surface density of cargo), and that detachment is a first
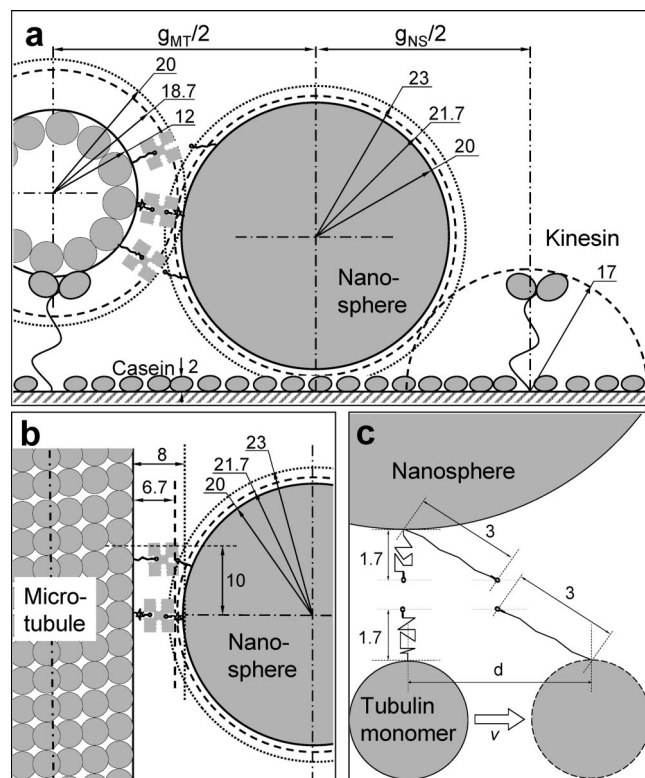

Figure 3. Geometry of the microtubule–nanosphere collision. (a) Cross section. The microtubule is elevated 17 nm above the substrate surface[18] and the nanosphere sits on a 2 nm casein layer.[32] The radius of a microtubule increases from 12 to 18.7 nm upon biotin–streptavidin functionalization and the radius of a nanosphere increases from 20 to 21.7 nm upon biotinylation. The flexible biotin linker confers an average boundary (dashed lines) and a limiting boundary (dotted lines) on the supramolecular structures. (b) Top view. A second biotin–streptavidin–biotin connection can only be established from a neighboring tubulin dimer if the biotins are almost fully extended, which is a rare event. (c) A biotin–streptavidin–biotin connection formed upon initial contact can strengthen while the biotin linkers are extended to their full contour length as the microtubule moves a distance $d = 5$ nm.

order reaction (rate proportional to sites loaded per microtubule). The data set for each experiment was fitted by the equation

$$N = \frac{k_{on}}{k_{off}}[1 - \exp(-k_{off}t)] \quad (1)$$

where k_{on} is the attachment rate, and k_{off} is the detachment rate.

Since the attachment occurs only via surface collisions, the attachment rate, k_{on} can be expressed as a product of rate of collision between a microtubule and nanospheres, k_{MT-NS}, and the sticking probability for each collision, S_{MT-NS}:

$$k_{on} = k_{MT-NS}S_{MT-NS}(v) = \sigma_{NS}g_{MT}vS_{MT-NS}(v) \quad (2)$$

where the nanosphere surface density σ_{NS} and gliding velocity v are directly measured and the grasp g_{MT} of the microtubule is estimated to be 80 nm based on the geometry of the kinesin-bound microtubule[18] and nanosphere (Figure 3c).
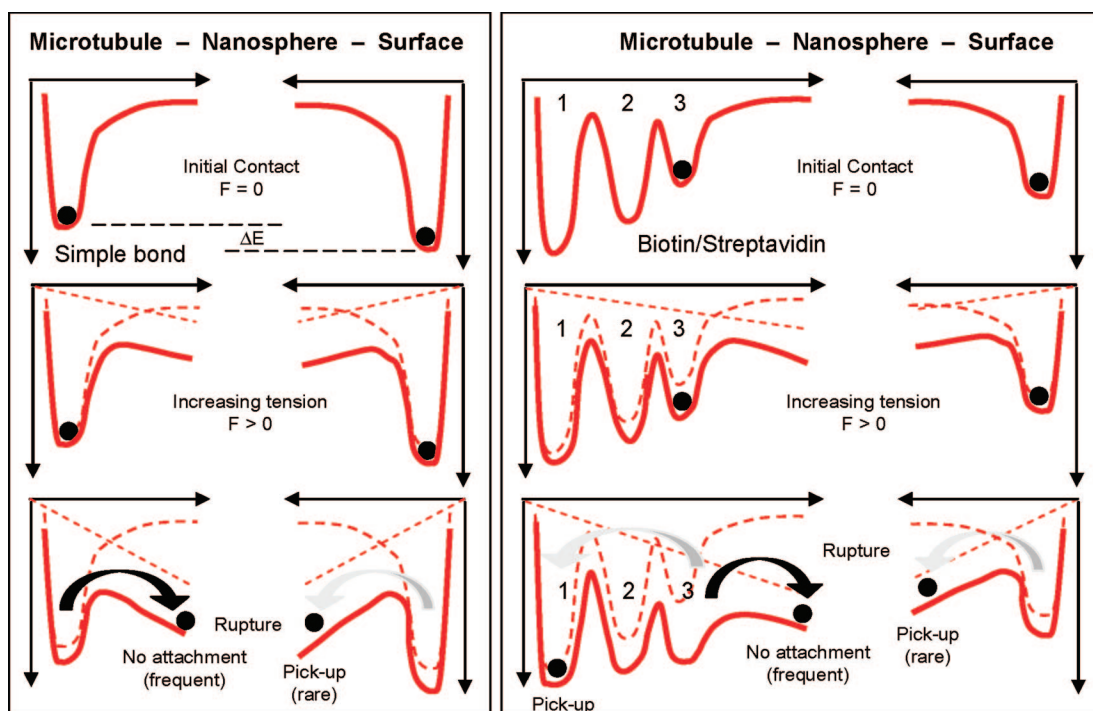
Figure 4. Schematic of the unbinding process. (Left) The formation of a microtubule/nanosphere linkage via a simple bond with a single potential energy minimum can reproduce the frequency of attachment but not the dependence on microtubule velocity, which determines the time of contact. (Right) The formation of a microtubule/nanosphere linkage via a biotin/streptavidin bond, which strengthens over time by transitioning into more tightly bound states, causes the increase in binding probability with increasing time of contact.

Sticking is a result of the repeated attempts of streptavidins attached to the microtubule to grasp the biotinylated nanosphere, and $S_{MT\text{-}NS}$ is thus given by

$$S_{MT-NS}(v) = 1 - [1 - P_{on}(v)]^n \qquad (3)$$

where $P_{on}(v)$ is the velocity-dependent probability that a linkage is successfully formed during an individual biotin−streptavidin encounter, and n is the number of encounters.

The number of encounters n is given by the product of the number of streptavidins on the microtubule simultaneously within reach of the biotin linkers on the nanosphere, the number of tubulin dimers along the length, and the probability that a tubulin dimer carries a streptavidin.

To estimate the number of simultaneous streptavidin−biotin contacts, we examine the details of the interface between microtubule and nanosphere (Figure 3). Both are covered with a layer of biotin whose thickness is equal to the most probable end-to-end distance of the flexible linker (1.7 nm, biotin-XX). The microtubule is further coated with streptavidin, adding another 5 nm to its radius. The most-probable boundary of the microtubule-biotin−streptavidin (MBS) structure and the biotinylated nanosphere are represented by the dashed lines. Because of Brownian motion, the biotin linkers can extend up to their full contour length (3 nm) and move the boundary of the MBS structure as well as the boundary of the biotinylated nanospheres to the dotted line. Contact between a MBS structure and the biotinylated nanosphere is established at the most probable configuration (contact of dashed lines). We conclude that streptavidins on neighboring protofilaments (cross-section, Figure 3a) cannot be simultaneously in contact with the biotinylated nanosphere

even when the biotin linkers are fully extended. Along the same protofilament (axial direction, Figure 3b), the two neighboring streptavidins can be simultaneously in contact. However, the biotins on both, the microtubule and the nanosphere, would have to be extended to 90% of their contour lengths for these additional contacts to be established. The probability of this is small, and thus the contribution of these streptavidins to the overall attachment of the biotinylated nanosphere can be neglected.

Hence, approximately one streptavidin on the microtubule interacts with the biotinylated nanosphere at a given instant. By measuring the average length of the microtubules (4.5 ± 0.4 μm) and the biotinylation ratio of the tubulin (0.6 ± 0.1 biotins per tubulin dimer with a length of 8 nm), we determined that in average, $n = 340 \pm 90$ attempts to form a linkage were made during each collision between a microtubule and a nanosphere.

The duration of each biotin−streptavidin contact, t_c, is calculated from the microtubule velocity and the distance d = 5 nm that the MBS structure moves from the initial contact with the stationary nanosphere until the biotin linkers have extended up to their full contour length (Figure 3c) and either rupture of the connection or attachment of the nanosphere have to occur.

We propose that the velocity dependence of P_{on}, which decreases from 35×10^{-4} to 7×10^{-4} as $S_{MT\text{-}NS}$ decreases from 0.7 at 50 to 0.2 at 400 nm/s, can be understood by considering the kinetics of the attachment process. In the attachment process, the newly formed biotin−streptavidin bond competes with the nonspecific attachment of the
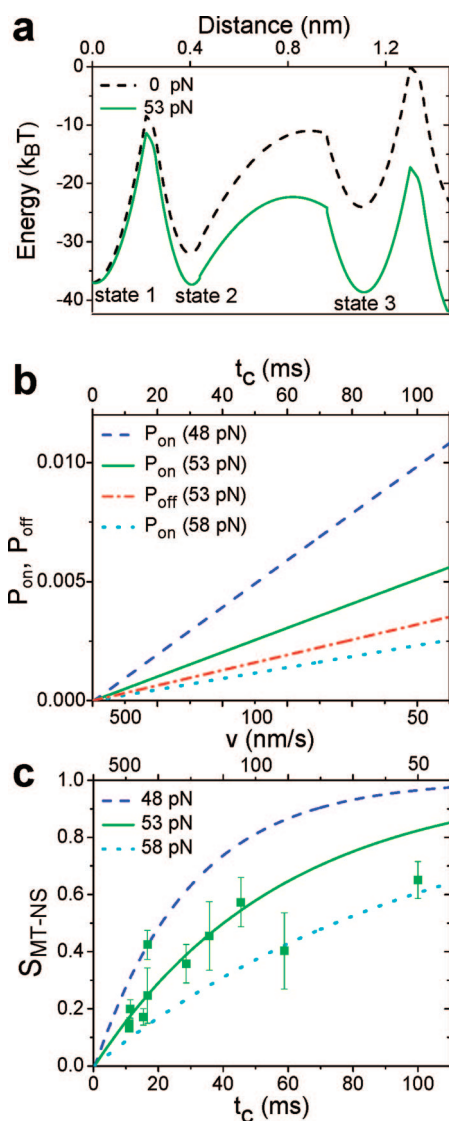
Figure 5. (a) The potential energy landscape of the biotin−streptavidin bond as determined by Pincet et al. in the absence of a force (dotted black curve) and in the presence of a 53 pN opposing force (solid green curve). (b) P_{on}. Probability for a biotin−streptavidin bond that is initially in the outermost minimum state 3 to transition to the equilibrium binding state 1 during the time of contact (green solid, 53 pN; blue dashed, 48 pN; turquoise dotted, 58 pN). P_{off}. Probability to transition out from the equilibrium binding state 1 in the presence of a 53 pN opposing force (red dash-dot). (c) The sticking probability S_{MT-NS} as a function of time of contact of each bond observed in experiments (green squares) and theoretically calculated for different opposing forces (lines).

nanosphere to the surface. The force exerted by the moving microtubule makes unbinding favorable for both bonds, and the outcome of the process (rupture of the biotin/streptavidin bond or the nanosphere/surface connection) is determined by the relative height of the two energy barriers to unbinding (Figure 4). The small probability of attachment ($P_{on} < 0.01$) implies that the newly formed biotin−streptavidin connection is weaker, or in other words that its activation energy to unbinding is 5−7 kT smaller compared to the nanosphere−surface connection.

If both linkages would be adequately represented by potentials with a single energy minimum, it would be

possible to specify potentials that result in a desired value of P_{on}, for example, 35×10^{-4}. However, a reduction in microtubule velocity, which increases the time available to complete the attachment process, would provide more time for the weaker of the two bonds to overcome the barrier to rupture. Thus, a decreasing velocity would not result in the observed increase in the attachment probability. Instead, we propose that the velocity dependence of P_{on} (and hence of S_{MT-NS}) is a result of the unusual shape of the biotin−streptavidin potential energy surface together with the varying time of contact t_c between biotin and streptavidin, which depends inversely on the microtubule velocity and is on the order of milliseconds.

Biotin−streptavidin linkages which are allowed to form over long periods of time are stronger than linkages which are subjected to pulling forces immediately after formation.[19] This results from the shape of the biotin−streptavidin energy landscape, which displays two metastable states in addition to the energy minimum (Figure 5a).[20] Contact between biotin and streptavidin initially populates the outermost state (state "3"), but a fraction of the population can overcome the barriers and reach the more stable equilibrium state (state "1"). We assume that only these stronger bonds can overcome the nonspecific adhesion of the nanosphere to the surface and contribute to nanosphere attachment to the microtubule, meaning that the attachment probability P_{on} is equal to the probability to transition from state 3 to state 1.

To calculate the fraction of the encounters leading to the formation of a strong biotin−streptavidin bond (and attachment), we solve the time-dependent master equation governing the population of states 1, 2 and 3 using the potential energy surface parameters provided by Pincet et al.[19] (see Supporting Information). We assume that all bonds are initially in state 3 and that the potential energy surface is modified by a constant opposing force provided by the kinesin motors and balanced by the adhesion of the nanosphere to the surface. An opposing force of 53 ± 5 pN yields an excellent fit of the calculated velocity-dependence of the sticking probability S_{MT-NS} to the experimental data (Figure 5c).

Of course, a constant force does not accurately reflect the complex variation of the force exerted on the newly formed biotin−streptavidin bond over time. However, the calculated linear dependence of the population of state 1 (and the attachment probability P_{on}) on the time of contact t_c is simply a result of the small probability of overcoming the two barriers and not a result of the assumed force profile (Figure 5b). In other words, changing the force profile affects the value of the force providing the best fit, but not the shape of the calculated dependence of S_{MT-NS} on velocity (Figure 5c).

Each microtubule has on average 11 motors attached to it, based on the measured average length of 4.5 ± 0.4 μm and a functional motor density of 100 μm^{-2} (determined by landing rate measurements[21]). These 11 motors can provide a force of ∼50 pN at a stepping velocity one third of the unloaded velocity,[22] if a linear scaling of force generation with motor number is assumed.[23] The nonspecific adhesion between the nanosphere and the surface can also readily

provide a counteracting force of 50 pN for a few milliseconds, considering the force tolerances of typical noncovalent bonds.[24] We thus conclude that the velocity-dependence of the sticking probabilities is indeed a result of the time-dependent strength of the biotin−streptavidin interaction.

The detachment rate can similarly be modeled as a product of the rate of collision between the loaded nanosphere and nanosphere binding sites on the surface, and the probability of unbinding in each collision. The unbinding probability per collision is twice the rupture probability of a biotin/streptavidin bond at the specified force, since two biotin/streptavidin bonds connect the nanosphere to the microtubule.

Because nanospheres bind only to kinesins on the surface, a collision occurs if the loaded nanosphere encounters functional motors (present at a density[21] of $\sigma_{kin} = 100\ \mu m^{-2}$ exerting an average force of 53 pN as in the loading process) or defective motors (present at a density[25] of $\sigma'_{kin} = 0.5\ \mu m^{-2}$). Defective motors must be able to bind to microtubules very tightly, since the binding of a gliding microtubule to a defective motor results in buckling of the microtubule[26] and spiraling.[27,28] We assume that the binding of nanospheres to defective motors is at least 3-fold stronger than the binding to functional motors, causing the unbinding probability to be close to unity.

Active and defective motors thus make independent contributions to the detachment rate

$$k_{off} = 2v\langle g_{NS}\rangle[\sigma_{kin}P_{off}(53pN, v) + \sigma'_{kin}] \tag{4}$$

The calculation of the distance g_{NS} over which a nanosphere loaded onto a microtubule can grasp a kinesin is complicated by the fact that the gliding microtubule likely rotates around its axis[29] placing the nanosphere out of reach for roughly half the time. A detailed calculation yields $<g_{NS}>$ equal to 33 nm (Figure 3a; details in Supporting Information). The velocity-dependent detachment probability for encounters with functional motors P_{off} is again assumed to be equal to the probability of escape from the equilibrium binding state 1 of the biotin−streptavidin binding potential energy surface at time t_c (Figure 5b). The calculated unbinding rate k_{off}, combining the velocity-independent contribution from encounters with active motors and the linearly increasing contribution from encounters with defective motors, fits the observed data effortlessly (Figure 2f).

Our attachment and detachment rate model allows us to predict the loading behavior for microtubules which use biotin−streptavidin chemistry and surface attachment of cargo as the loading mechanism (Figure 6). The predicted loading rises linearly from zero with increasing velocity, reaches a maximum at a velocity of ∼200 nm/s, and falls to 75% of the maximum at the top speed of the molecular shuttle. The predicted loading behavior matches the experimental data scaled to a constant nanosphere density.

The existence of an optimal velocity for cargo attachment to molecular shuttles is a consequence of the complex binding energy landscape of the biotin−streptavidin linkages. The behavior of biotin−streptavidin linkages is best captured by the "glue" metaphor, which emphasizes that a certain curing
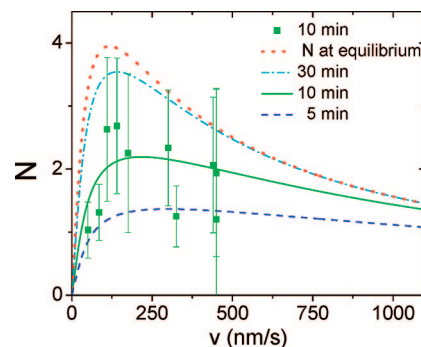

Figure 6. Predicted microtubule loading. The attachment and detachment model are used to predict loading as function of microtubule velocity at different times after bead injection. The on- and off-rates were calculated assuming a nanosphere density of 1 μm^{-2}. Experimental values at 10 min after nanosphere injection (green squares) were also normalized to a nanosphere density of 1 μm^{-2}.

time is required to achieve the ultimate strength of the linkage. In contrast, lectin−selectin or mannose−FimH catch bonds function as "hooks" that gain strength under load, DNA−DNA linkages act like "adhesive tape", and Nickel/His-tag linkages resemble "magnets". Translating the description of molecular building blocks and their behavior into appropriate metaphors is important for the design and understanding of nanosystems, since it enables the correct application of our engineering intuition honed by decades of experience with macrosystems.

Materials and Methods. The experiments were performed in an approximately 100 μm high and 1 cm wide flow cells assembled from two coverslips and double-stick tape.[30] First, a solution of casein (0.5 mg/mL, Sigma) dissolved in BRB80 (80 mM PIPES, 1 mM MgCl$_2$, 1 mM EGTA, pH 6.9) was injected into the flow cell. After 5 min, it was exchanged with a kinesin solution (∼10 nM in BRB80 with 0.5 mg/mL casein and varying ATP concentration). Five minutes later, this was exchanged against a motility solution (an antifade system made up of 20 mM D-glucose, 20 $\mu g/mL$ glucose oxidase, 8 $\mu g/mL$ catalase, 10 mM dithiothreitol, and ATP at concentrations from 20 μM to 1 mM in BRB80) containing 0.8 $\mu g/mL$ biotinylated microtubules. Five minutes were allowed for microtubule attachment after which 20 nM Alexa568-labeled streptavidin (Molecular Probes) in motility solution was perfused into the flow cell and incubated for five minutes to cover all the biotin sites on the microtubules.[16] Finally, after three washes with motility solution, biotin-labeled 40 nm nanospheres loaded with fluorescein dye (Molecular Probes Inc.) at different concentrations (25−100 pM) in motility solution were introduced into the flow cell. The flow cell was mounted on the microscope stage and the time elapsed since nanosphere introduction was recorded. An Eclipse TE2000-U fluorescence microscope (Nikon, Melville, NY) equipped with a 100× oil objective (NA 1.45), an X-cite 120 lamp (EXFO, Ontario, Canada), a FITC filter cube (no. 48001), a TRITC filter cube (no. 48002, Chroma Technologies, Rockingham, VT), and an iXon EMCCD camera (ANDOR, South Windsor, CT) was used to image microtubules and nanospheres on the bottom surface of flow

cells. The exposure time was 0.5 s, while the time between exposures was varied from 4 to 8 s depending on microtubule speeds. Uninhibited transport of nanosphere-loaded microtubules at nanosphere concentrations as high as 1 nM was observed if the excitation light intensity was reduced from 2.1 to 0.1 mWcm^{-2}, indicating that the previously described limit[10] of 10 pM is a result of photodamage.

Kinesin and microtubules. A kinesin construct consisting of the wild-type, full-length *Drosophila melanogaster* kinesin heavy chain and a C-terminal His-tag was expressed in *Escherichia coli* and purified using a Ni-NTA column.[31] Microtubules were prepared by polymerizing 20 μg of biotin labeled-tubulin (Cytoskeleton Inc., Denver CO) in 6.5 μL of growth solution containing 4 mM MgCl$_2$, 1 mM GTP, and 5% DMSO (v/v) in BRB80 buffer for 30 min at 37 °C. The microtubules with lengths between 1 and 20 μm were 100-fold diluted and stabilized in 10 μM Paclitaxel (Sigma, Saint Louis MO). A biotin quantitation kit (Invitrogen Inc.) was used to determine that there are 0.6 ± 0.1 moles of biotin per mole of tubulin.

Supporting Information Available: This material is available free of charge via the Internet at http://pubs.acs.org.

References

(1) Hess, H.; Vogel, V. *Rev. Mol. Biotechnol.* **2001**, *82* (1), 67–85.
(2) van den Heuvel, M. G. L.; Dekker, C. *Science* **2007**, *317* (5836), 333–336.
(3) Hess, H.; Clemmens, J.; Qin, D.; Howard, J.; Vogel, V. *Nano Lett.* **2001**, *1* (5), 235–239.
(4) Diez, S.; Reuther, C.; Dinu, C.; Seidel, R.; Mertig, M.; Pompe, W.; Howard, J. *Nano Lett.* **2003**, *3* (9), 1251–1254.
(5) Bachand, G. D.; Rivera, S. B.; Boal, A. K.; Gaudioso, J.; Liu, J.; Bunker, B. C. *Nano Lett.* **2004**, *4* (5), 817–821.
(6) Patolsky, F.; Weizmann, Y.; Willner, I. *Nat. Mater.* **2004**, *3* (10), 692–695.
(7) Mansson, A.; Sundberg, M.; Balaz, M.; Bunk, R.; Nicholls, I. A.; Omling, P.; Tagerud, S.; Montelius, L. *Biochem. Biophys. Res. Commun.* **2004**, *314* (2), 529–534.
(8) Bachand, M.; Trent, A. M.; Bunker, B. C.; Bachand, G. D. *J. Nanosci. Nanotechnol.* **2005**, *5* (5), 718–722.
(9) Boal, A. K.; Bachand, G. D.; Rivera, S. B.; Bunker, B. C. *Nanotechnology* **2006**, *17* (2), 349–354.
(10) Kato, K. A.; Goto, R.; Katoh, K.; Shibakami, M. *Biosci., Biotechnol., Biochem.* **2005**, *69* (3), 646–648.
(11) Hirabayashi, M.; Taira, S.; Kobayashi, S.; Konishi, K.; Katoh, K.; Hiratsuka, Y.; Kodaka, M.; Uyeda, T. Q. P.; Yumoto, N.; Kubo, T. *Biotechnol. Bioeng.* **2006**, *94* (3), 473–480.
(12) Taira, S.; Du, Y. Z.; Hiratsuka, Y.; Konishi, K.; Kubo, T.; Uyeda, T. Q. P.; Yumoto, N.; Kodaka, M. *Biotechnol. Bioeng.* **2006**, *95* (3), 533–538.
(13) Bachand, G. D.; Rivera, S. B.; Carroll-Portillo, A.; Hess, H.; Bachand, M. *Small* **2006**, *2* (3), 381–385.
(14) Ramachandran, S.; Ernst, K.-H.; Bachand, G. D.; Vogel, V.; Hess, H. *Small* **2006**, *2* (3), 330–334.
(15) Brunner, C.; Wahnes, C.; Vogel, V. *Lab Chip* **2007**, *7* (10), 1263–1271.
(16) Thomas, W. E.; Trintchina, E.; Forero, M.; Vogel, V.; Sokurenko, E. V. *Cell* **2002**, *109* (7), 913–923.
(17) Marshall, B. T.; Long, M.; Piper, J. W.; Yago, T.; McEver, R. P.; Zhu, C. *Nature* **2003**, *423* (6936), 190–193.
(18) Kerssemakers, J.; Howard, J.; Hess, H.; Diez, S. *Proc. Natl. Acad. Sci. U.S.A.* **2006**, *103* (43), 15812–15817.
(19) Pincet, F.; Husson, J. *Biophys. J.* **2005**, *89* (6), 4374–4381.
(20) Pierres, A.; Touchard, D.; Benoliel, A.-M.; Bongrand, P. *Biophys. J.* **2002**, *82* (6), 3214–3223.
(21) Katira, P.; Agarwal, A.; Fischer, T.; Chen, H.-Y.; Jiang, X.; Lahann, J.; Hess, H. *Adv. Mater.* **2007**, *19*, 3171–3176.
(22) Visscher, K.; Schnitzer, M. J.; Block, S. M. *Nature* **1999**, *400* (6740), 184–9.
(23) Klumpp, S.; Lipowsky, R. *Proc. Natl. Acad. Sci. U.S.A.* **2005**, *102* (48), 17284–9.
(24) Schmidt, J. J.; Jiang, X.; Montemagno, C. D. *Nano Lett.* **2002**, *2* (11), 1229–1233.
(25) Nitta, T.; Hess, H. *Nano Lett.* **2005**, *5* (7), 1337–1342.
(26) Gittes, F.; Meyhofer, E.; Baek, S.; Howard, J. *Biophys. J.* **1996**, *70* (1), 418–29.
(27) Weiss, D. G.; Langford, G. M.; Seitz-Tutter, D.; Maile, W. *Acta Histochem.* **1991**, *41*, 81–105.
(28) Bourdieu, L.; Duke, T.; Elowitz, M. B.; Winkelmann, D. A.; Leibler, S.; Libchaber, A. *Phys. Rev. Lett.* **1995**, *75* (1), 176–179.
(29) Nitzsche, B.; Ruhnow, F.; Diez, S. *Nat. Nanotechnol.* **2008**, *3*, 552–556.
(30) Howard, J.; Hunt, A. J.; Baek, S. *Methods Cell Biol.* **1993**, *39*, 137–47.
(31) Coy, D. L.; Wagenbach, M.; Howard, J. *J. Biol. Chem.* **1999**, *274* (6), 3667–71.
(32) Fragneto, G.; Thomas, R. K.; Rennie, A. R.; Penfold, J. *Science* **1995**, *267* (5198), 657–660.

NL803831Y